Observation of the Dynamics of a Focal Spot Using a Long-Pulse Linear Induction Accelerator

Yu. A. Trunev, D. I. Skovorodin, A. V. Burdakov, S. S. Popov, P. A. Kolesnikov, V. V. Danilov, V. V. Kurkuchekov, M. G. Atlukhanov, I. V. Kulenko, A. S. Arakcheev, V. T. Astrelin, S. L. Sinitsky, A. A. Starostenko, D. A. Starostenko, O. A. Nikitin, V. Yu. Politov, and E. S. Lee

***Abstract*— A diagnostic has been developed to study the focusing dynamics of a high-power electron beam on a target. The diagnostic uses a pinhole camera to observe bremsstrahlung from the converter target. A data acquisition system yields images of the beam focal spot with a frame duration of 20 ns and an almost unlimited recording duration. The focal spot dynamics of a linear induction accelerator with an energy of 1.5 MeV, a current of 1.2 kA and a pulse duration of 350 ns were studied. The focal spot was found to be disrupted within the first 100 ns of the pulse. Defocusing has a complex 3-D character. The feasibility of additional cleaning of the target using an accelerator pre-pulse was shown. Stable beam focusing for up to 200 ns was demonstrated.**

***Index Terms*— Beam defocusing, beam diagnostic, ion backstream, linear induction accelerator (LIA), pinhole, time-resolved spot size.**

I. Introduction

LINEAR induction accelerators (LIAs) of electrons have found applications in applied problems [1] and fundamental research for the production of warm dense matter [2]. In these applications, a strong focusing of the beam on the target surface is required. High beam quality in a linear accelerator enables focusing the beam into a spot with a diameter about 1 mm. Strong focusing leads to a high density of deposited energy in the target, in the range of 1–100 eV/atom, which results in the formation of plasma on the target surface [3], [4]. In a number of experimental works [5], [6], the target plasma was shown to become an ion emitter. The electric self-field of the electron beam leads to the pulling of ions and the formation of a back stream. The space charge of the ions upsets the balance of forces in the beam and leads to its rapid defocusing in a matter of tens of nanoseconds. This phenomenon hampers obtaining a high-quality beam focus on the target. The defocusing rate depends on the ions species in the back stream. The surface plasma is formed not only from the target material but also from the contaminations adsorbed on the surface, obviously, due to their lower mass, lighter ions from water, and hydrocarbons spread into the beam more rapidly. The effect of target surface quality on beam focusing was studied in [7]. To reduce the rate of beam defocusing on the target, it was proposed [8], [9] to clean the surface in advance using a high-power laser pulse.

There are several methods for directly observing beam defocusing. One of them is by the registration of Cherenkov radiation from a dielectric plate (or fiber) on the beam path [7], [10]. However, the use of bremsstrahlung gamma rays from the target itself better addresses the needs of applied problems [11], [12]. By measuring the dynamics of the X-ray source, one can track the focal spot on the target. In this case, the X-ray source dynamics depends on the radiation transport process, plasma process, and hydrodynamics of the target. The observation technique is based on projecting the X-ray flux from the target onto a scintillator using a pinhole camera or the roll-bar (knife edge) technique [13], [14]. There are several approaches to recording the dynamics of the scintillator glow. The most common one is based on the use of multiple cameras with fast shutters [11], [12], [15], [16]. In this case, the light leaving the scintillator is divided between the cameras, which take pictures at different points of time. Thus, the dynamics of the focal spot is recorded. Usually, the fast shutter is an image intensifier located in front of the camera matrix. Another approach relies on the use of optical fibers to bring the light from the scintillator to photomultipliers or photodiodes [17]–[21]. There are also hybrid techniques, which combine both methods [22]–[24]. Using multiple cameras with fast shutters makes it possible to achieve good spatial resolution. However, in this case, the number of frames that can be made during one accelerator pulse is restricted. The latter approach is free of this limitation.

In this article, we investigate beam defocusing in an accelerator with an energy of 2 MeV and a pulse duration of up to 300 ns. A relatively low beam energy and a long pulse duration are unfavorable for obtaining a stable focal spot [25]. On the other hand, these are the beam parameters that are convenient to study the effect of the target plasma, because with them,

Manuscript received September 4, 2019; revised January 29, 2020 and April 14, 2020; accepted April 20, 2020. Date of publication May 14, 2020; date of current version June 10, 2020. The review of this article was arranged by Senior Editor C. A. Ekdahl. *(Corresponding author: Yu. A. Trunev.)*

Yu. A. Trunev, D. I. Skovorodin, A. V. Burdakov, S. S. Popov, V. V. Danilov, V. V. Kurkuchekov, M. G. Atlukhanov, I. V. Kulenko, A. S. Arakcheev, V. T. Astrelin, S. L. Sinitsky, A. A. Starostenko, and D. A. Starostenko are with the Budker Institute of Nuclear Physics, Siberian Branch Russian Academy of Sciences, 630090 Novosibirsk, Russia (e-mail: yu.a.trunev@inp.nsk.su).

P. A. Kolesnikov, O. A. Nikitin, V. Yu. Politov, and E. S. Lee are with the Federal State Unitary Enterprise Russian Federal Nuclear Center—Academician E. I. Zababakhin All-Russian Research Institute of Technical Physics, 456770 Snezhinsk, Russia (e-mail: vniitf@vniitf.ru).

Color versions of one or more of the figures in this article are available online at http://ieeexplore.ieee.org.

Digital Object Identifier 10.1109/TPS.2020.2991841

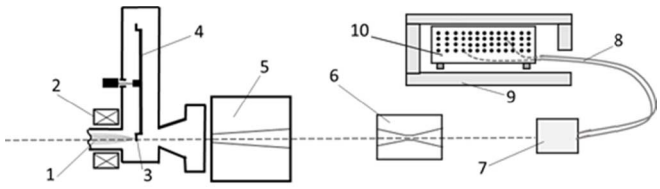

Fig. 1. Schematic of the experiment (top view). 1—LIA-focused electron beam; 2—final magnetic lens; 3—tantalum target; 4—rotating target holder; 5—lead collimator; 6—conical pinhole camera; 7—scintillation detector; 8—optic fiber bundle; 9—EMI and lead shield; 10—DAQ recording system.

it manifests most clearly. The observation of the focal spot on the target was performed using a 64-channel multipixel detector, which allows taking frames every 20 ns. This article presents a brief description of a diagnostic and the results of the focal spot measurement. The feasibility of cleaning the target surface with a special prepulse was explored.

II. Experimental Installation and the Diagnostic

The experiments were carried out using an LIA [26] with an accelerating voltage of about 1.5 MV. The beam current was about 1.2 kA with a base pulsewidth of 350 ns. Four solenoidal magnetic lenses transported the beam to the target. Three identical pulse lenses focused the beam in the transport line. The final lens focused the beam on a tantalum target. The parameters of the accelerated beam were measured after the diode and at the entry to the target chamber by a standard set of diagnostics: capacitive dividers, beam position monitors, and current transformers.

A schematic of the experiment is shown in Fig. 1. The final lens focused the accelerated electron beam on a tantalum plate (the target). The targets were mounted in a circle on a rotating holder. According to [27], the optimal thickness of a Ta target for a 2-MeV beam is about 0.036 cm, but such a thin target is not mechanically strong. Moreover, when the LIA operates in double-pulse mode, the first pulse blows off part of the target material. Thus the effectiveness of the second shot depends on the remaining thickness of the material. For this reasons, we used two Ta targets: one with 0.4 mm thick and the other, 1 mm. All targets were duly prepared before installed in the target chamber: they were cleaned and annealed in vacuum before neatly mounted on the holder in such a manner as to minimize accidental contamination. The bremsstrahlung radiation produced by the beam in the target left the accelerator through an aluminum exit window. A massive lead collimator suppressed the parasitic (scattered) gamma radiation. It was 200 mm in thickness and the central hole was 10 mm in radius. The dynamics of the focal spot on the target was recorded using an original diagnostic based on a multipixel scintillation detector. The diagnostic consisted of a pinhole camera, a detector, and a multichannel digital data acquisition (DAQ) system. The tapered hyperbolically shaped pinhole camera was made of tungsten. The total length of the camera body was 100 mm. The minimum hole diameter was 0.6 mm. The pinhole had an angle of view of 6°. The point spread function (PSF) of the pinhole camera had been measured previously in separate experiments. The PSF is well approximated by a Gaussian function with a full width at half maximum (FWHM) of 0.8 mm. The pinhole camera projected the time-varying image of the X-ray spot on the target into the plane of the detector. The pinhole camera and the detector were aligned along the geometrical axis of the accelerator using a laser. The distance between the face plane of the detector and the target plane was 2.5 m. The pinhole camera and the detector were spaced so as to obtain a geometric magnification of 5. The detector body was a bronze matrix with 64 holes arranged in an 8×8 rectangular array. The holes contained plastic scintillation fibers, each of 3 cm in length and 1 mm in diameter. The scintillation decay time was $\sim$3 ns. The pitch between the centers of any two neighboring scintillators was 2 mm. Each scintillator was connected by an optical fiber with the corresponding channel of the DAQ system. Each optical fiber was about 6 m in length. The recording system consisted of photodiodes with a transimpedance amplifier coupled with a multichannel ADC. The recording system had a sampling frequency of 50 MHz, which ensured a frame duration of 20 ns. To be protected from electromagnetic interference (EMI/RFI) and intense background X-rays, the DAQ system was placed in a shielded rack with a lead shield around it.

III. Experimental Results

A. Beam Focus Measurement

The beam focus measurement procedure consisted of three stages. Typical signals at stages 1 and 3 are shown in Fig. 2. At the first step, the relative sensitivity of the detector channels was measured. For this purpose, the pinhole camera was removed and homogeneous illumination was recorded. X-ray was attenuated by a thin lead plate with a thickness of about 2 cm. It helps overcome the off-scale of the DAQ output signals. The waveforms [see Fig. 2(a)] could be interpreted as the total X-ray output of the LIA. For comparison, Fig. 2(a) shows a normalized LIA current from a current transformer installed before the target chamber.

At the second stage, the parasitic background was measured. The output window of the collimator was overlapped with a massive lead brick. One of the main sources of the background signal was the Cherenkov glow in a transport optical fiber [28]. The relative sensitivity of the detector channels was found after the subtraction of the background signals from the homogeneous illumination signals. Then, the signal amplitude was averaged over a time close to the duration of the X-ray flash (the beam pulse). The result was an array of 64 coefficients of the relative sensitivity of the detector channels.

At the third stage, the lead brick was removed, the pinhole camera was returned to its place, and the beam focus on the target was measured. Fig. 2(b) shows several waveforms of edge pixels with near to "zero" amplitude (i.e. channels-pixels of the "background"). The waveforms of several peripheral pixels—that is, pixels of the beam "halo"—are shown in Fig. 2(c). Fig. 2(d) shows the waveforms with the maximum amplitude, i.e. the pixels of the beam center. In this shot, the beam current was 1.2 kA and the total energy was 1.5 MeV. The target was a tantalum plate 0.4 mm thick.

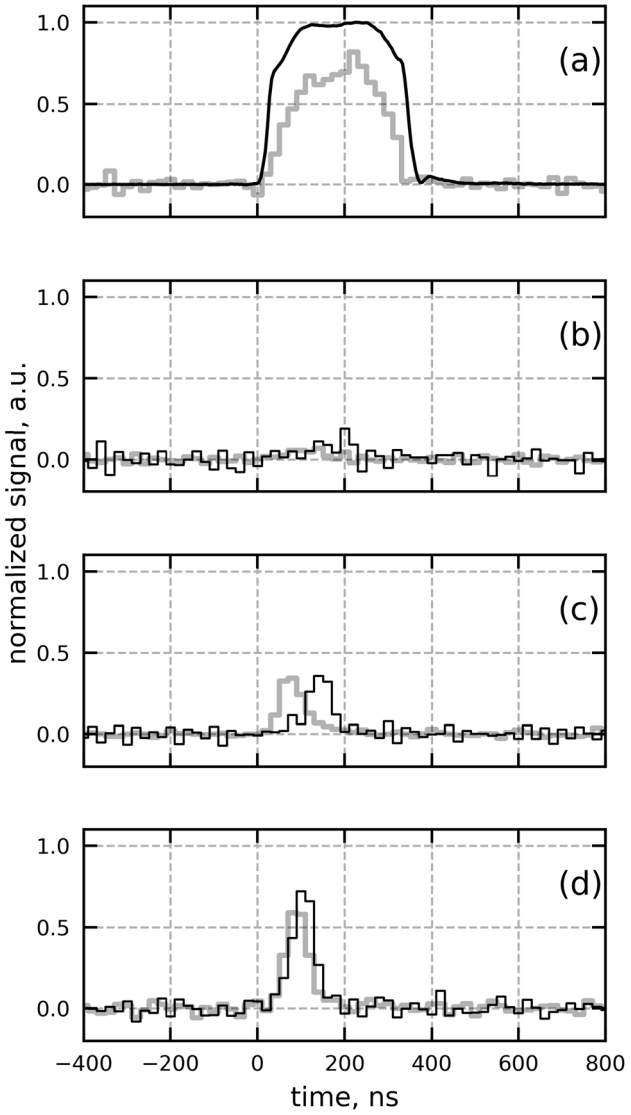

Fig. 2. Typical waveforms of the photocurrent from DAQ channels. (a) Gray step plot: total X-ray output measured without the pinhole; black solid line: beam current measured by a current transformer. (b) Black and gray step plots: respective responses of two opposite "edge" pixels. (c) Black and gray step plots: respective responses of two opposite "halo" pixels. (d) Black and gray step plots: respective responses of two neighboring center pixels.

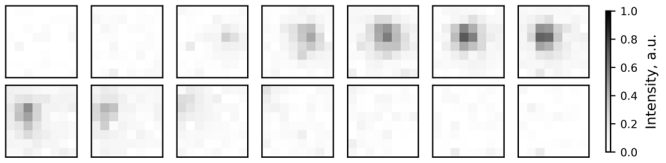

Fig. 3. Sequence of snapshots of the beam focus on the target from 0 to 260 ns, with a 20-ns exposure. A typical shot onto the unpretreated 0.4-mm-thick target.

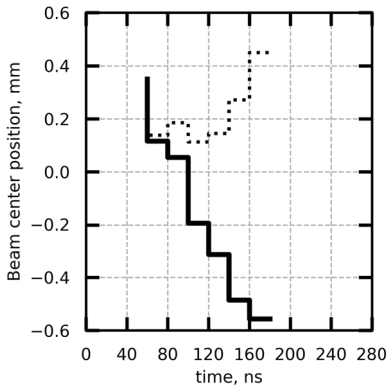

Fig. 4. Beam center position versus time for the shot corresponding to snapshots presented in Fig. 3. Dotted line: vertical direction; solid line: horizontal direction.

The signals obtained using the DAQ system [see Fig. 2(b)–(d) for typical signals] were converted into an array with two axes: amplitudes (versus time) and pixel numbers. Further, the array was normalized to the matrix of sensitivity coefficients of the channels, with the contribution of the parasitic background taken into account.

Then the data array was transformed into time sequences of frames with a time step equal to the DAQ sampling rate. Each frame consisted of an array of 8×8 pixels. All pixels were placed in the image in the same sequence as they were located on the scintillation matrix of the detector. Fig. 3 shows a sequence of frames recorded by the detector in the shot given above in Fig. 2. The intensity of each pixel was normalized to the maximum amplitude in proper series of shots (the maximum amplitude of a one-day experimental run). In addition to visualization in the form of frames, we characterized the beam profile in each frame with its average parameters. The position of the beam focus was found as the average weighted by the pixel intensity along the horizontal x-axis and the vertical y-axis. The characteristic size of the beam focus on the target was determined only in the frames where the beam was already formed and fit into the size of the detector. The beam focus profile was approximated by 2-D Gauss function. The characteristic size was taken as the full width at half-maximum, as in [13]. In that case, the width of the PSF of the pinhole was subtracted from the width of the spot. Fig. 4 shows the position of the beam center during the beam pulse. The center position was calculated from the shot shown in Fig. 3.

B. What Happens When the Target Surface Is Cleaned

Figs. 2(d) and 3 show that only one part of the beam is focused on the target. The focal spot was observed for 100 ns and then the beam was defocused. In [25], the interaction of the beam with various species of ions was studied using the PiC code KARAT. It was shown that a flow of hydrogen ions could destroy a 2-MeV beam in several tens of nanoseconds. If the target is sufficiently clean, dense tantalum plasma is still formed on its surface. The beam fields can also pull out tantalum ions. However, because these ions are heavy, it takes more than 100 ns for them to substantially affect the beam. A possible way to address ion backstreaming is by elimination of surface contamination before a shot.

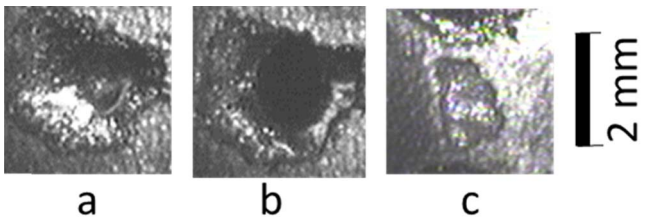

Fig. 5. Typical beam imprints on a 1-mm-thick tantalum target. (a) typical pulse, (b) hole, (c) melt-through from a pre-shot.

In [8] and [9] in order to reduce the rate of beam defocusing, precleaning of the target surface with a high-power laser pulse was proposed. This approach requires additional efforts to introduce high-power laser radiation to the target chamber and is associated with a number of obvious technical difficulties. At the same time, the LIA beam with an energy of 1.5 MeV does not destroy the target completely. Thus, we can use an accelerator shot for deep cleaning of the target surface.

However, the optimally tuned beam left a deep crater [see Fig. 5(a)]. Nevertheless, the next shot into the crater had better dynamics of the beam spot. It had higher intensity in center pixels of the detector. Moreover, beam focusing was conserved for up to 200 ns.

It should be noted that a 0.4–1-mm-thick tantalum target is really thick for a 1.5 MeV beam. There is strong self-absorption in the target of photons with energies below 300 keV. Thus, the ablation of the target surface can lead to an increase in X-ray yield. However, it seems that the dynamics of the X-ray spot during one pulse of the LIA is not affected by ablation of the target. In our case, the estimate of energy deposition in the target gives the expansion velocities in the order of magnitude of millions of centimeters per second. It should be taken into account that the energy deposition is distributed over the beam pulse. Moreover, the transit time of the unloading wave through the target material is only a few times shorter than the pulse duration. Thus, we assume that there is no substantial ablation of material during the beam pulse. This is confirmed by the absence of any sharp change in the behavior of the waveform corresponding to the total X-ray yield during the pulse [see Fig. 2(a)].

It is not clear what temperature of the target should be reached to have the surface cleaned. Apparently, the temperature should be sufficiently high not only for removal of adsorbed gases, but also for decomposition of persistent compounds on the surface of the tantalum target and for elimination of the gas dissolved in the surface layer of the target. For this reason, a special series of experiments was carried out. In that sequence of shots, an optimal mode was chosen for cleaning the target surface. We used the detector to control the quality of beam focusing on the target. During this experimental run, two consecutive shots were made to the same point on the target with a characteristic spacing of a few minutes between them. The preparatory shot was made with either full or weakened current in the final lens. The second shot was always performed with a well-focused beam.

The main results of the experimental run are summarized in Fig. 6. Each curve represents the signal of a pixel in the center area of the detector with the maximum intensity in the corresponding shot. These curves were additionally normalized to the maximum amplitude in that experimental run. The curves for the total X-ray and LIA current in Fig. 6(a) are the same as in Fig. 2(a), to illustrate the total duration of the accelerator pulse. Fig. 5(b) shows two shots on the 1-mm-thick target. The gray curve is a shot on the unpretreated (that is, not preheated) target. The black curve shows a change in beam dynamics due to preheating the target with a strongly defocused beam. The current in the final lens was decreased so that the beam focus on the target was several centimeters in size. Then a sequence of several tens of shots with a frequency of 0.5 Hz was performed. Such preheating causes

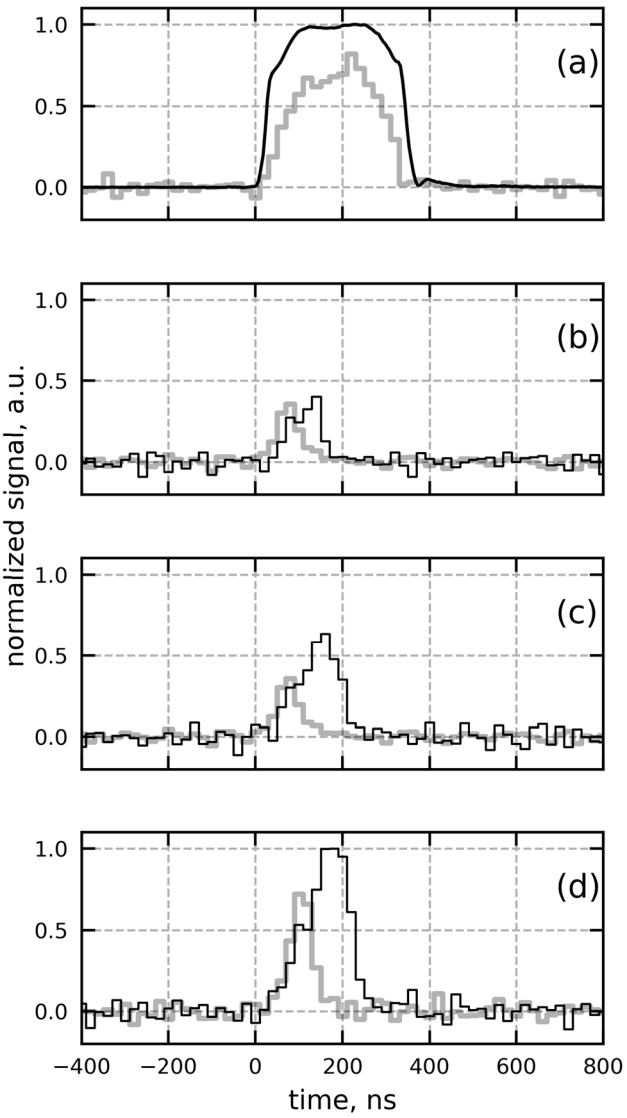

Fig. 6. Typical waveforms of the photocurrent from DAQ channels corresponding to a center pixel. (a) Gray step plot: total X-ray output measured without the pinhole; black solid line: beam current measured by the current transformer. (b) Black curve: shot on the point preheated by 10 pulses of an unfocused beam, gray curve: shot on the unpretreated 1-mm-thick target. (c) Black curve: shot on the pretreated 1-mm-thick target; gray curve: shot on the unpretreated 1-mm-thick target. (d) Black curve: shot on the pretreated 0.4-mm-thick target; gray curve: shot on the unpretreated 0.4-mm-thick target.

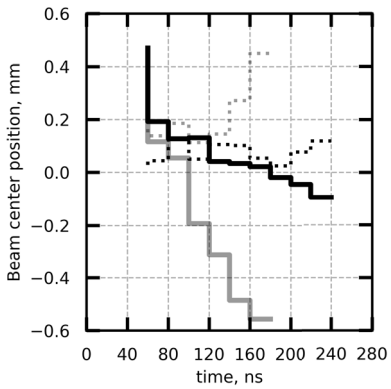

Fig. 7. Beam center position versus time for shots presented in Fig. 6(d). Dotted line: vertical direction; solid line: horizontal direction. Gray curves: beam center position as in Fig. 3; black curves: beam center position with the pretreated 0.4-mm-thick target.

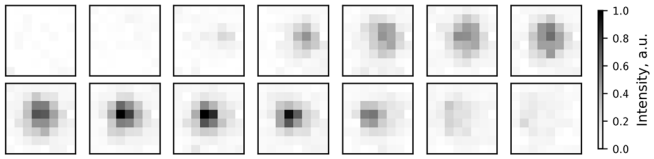

Fig. 8. Sequence of snapshots of the beam focus on the target from 0 to 260 ns, with 20-ns exposure. The shot to the pretreated 0.4-mm-thick target.

only minor changes to beam spot dynamics. An increase in the heating of the target by the pre-shot had virtually no effect before the target started melting. If the power density in the pre-shot was sufficient for solidified molten matter to appear on the target surface [Fig. 5(c)], it was concluded that the stability of the second shot was substantially improved. No further improvement in focusing during the preshot had any noticeable effect on the dynamics of the second shot. It is important to note that the cleaning effect persisted for several hours. It seems that the adsorption of gases on the melted tantalum surface was slow, because the residual vacuum in the accelerator was maintained at 10^{-8} Pa.

Fig. 6(c)–(d) shows the intensity of a center pixel after successful cleaning of two targets, one 0.4 mm and another 1 mm thick. Compared to the case presented in Fig. 6(b), the focus of the beam remained stable for a longer time. Cleaning also affects the dynamics of the position of the beam focus center (see Fig. 7, black curves). When the target is cleaned, the focus is virtually not drifting.

It is possible to obtain a well-focused beam on the target within 160–200 ns. This is illustrated in Fig. 8 describing the shot on the pretreated 0.4-mm-thick target. As can be seen, the duration of stable focusing increased more than twofold due to cleaning. However, the signal is still shorter than the signal of the total X-ray yield. Defocusing at times exceeding 200 ns might be associated with the formation of backstreaming ions of tantalum.

It should be noted that successful cleaning of the target does not require intense ablation, for which reason no noticeable decrease in the thickness of the target material is required either. Again, the cleaning effect lasts a finite time, which depends on the vacuum conditions. After tens of hours, the target was contaminated and the effect of target preparation wore off. Thus, we believe that the cleaning effect is associated with removal of surface impurities.

IV. Conclusion

A diagnostic to study the focusing dynamics of a high-power electron beam on a metal target has been developed. The diagnostic makes it possible to obtain images of the focal spot on a target with a 20-ns frame and a virtually unlimited total recording duration. Using this diagnostic, the dynamics of the focal spot produced by an electron beam from an LIA (1.5 MeV, 1.2 kA, 300 ns) was explored. With these beam parameters, the effect of the target plasma and the back stream of ions is the most pronounced. Despite a careful preparation and cleaning of the tantalum targets, the time during which a stable focus is observed does not exceed 100 ns. Not only is the beam defocused, but also the center of the spot drifts across the target surface.

The feasibility of additional cleaning of the target with a pre-pulse was explored. It was shown that an LIA pre-pulse allows the target surface layer to be purified. In order to reduce the damage to the target, the pre-pulse focus spot was increased. Beam focusing stability becomes substantially improved if the pre-pulse causes melting of the target surface. In this case, it is possible to obtain a stable beam focus that will persist for up to 200 ns. However, for the last 100 ns of the pulse the beam will stay defocused. Apparently, such behavior may be explained by the formation of backstreaming ions from tantalum itself.

Acknowledgment

The authors would like to thank Dr. A. D. Khilchenko and A. N. Kvashnin for the help in developing and tuning the multichannel digital data acquisition system.

References

[1] K. Peach and C. Ekdahl, "Particle beam radiography," *Rev. Accel. Sci. Technol.*, vol. 6, pp. 117–142, Jan. 2013, doi: 10.1142/s1793626813300065.

[2] J. E. Coleman and J. Colgan, "Spatially and temporally resolved measurements of a dense copper plasma heated by intense relativistic electrons," *Phys. Plasmas*, vol. 24, no. 8, Aug. 2017, Art. no. 083302, doi: 10.1063/1.4989797.

[3] V. B. Oliver, R. D. Welch, and P. T. Hughes, "Beam-target interactions in single- and multi-pulse radiography," MRC, London, U.K., Tech. Rep. MRC/ABQ-R-1909, Apr. 1999.

[4] A. C. L. Fontaine, "Ion emission at the target of the radiographic devices PIVAIR and AIRIX," *J. Phys. D: Appl. Phys.*, vol. 40, no. 6, pp. 1712–1732, Mar. 2007, doi: 10.1088/0022-3727/40/6/020.

[5] T. Houck, M. Garcia, and S. Sampayan, "Faraday cup measurements of the plasma plume produced at an X-Ray converter," in *Proc. 19th Intl LINAC Conf.*, Aug. 1998, p. 311.

[6] J. Zhu, H. Yu, X. Jiang, N. Cheng, and Y. Wang, "Target-plasma expansion induced by 20-MeV intense electron beam," *IEEE Trans. Plasma Sci.*, vol. 38, no. 10, pp. 2873–2876, Oct. 2010, doi: 10.1109/TPS.2010.2061869.

[7] C. Vermare, H. A. Davis, D. C. Moir, and T. P. Hughes, "Ion emission from solid surfaces induced by intense electron beam impact," *Phys. Plasmas*, vol. 10, no. 1, pp. 277–284, Jan. 2003, doi: 10.1063/1.1527629.

[8] Y. J. Chen *et al.*, "High intensity beam and X-Ray converter target interactions and mitigation," *AIP Conf. Proc.*, vol. 647, no. 1, pp. 240–254, Dec. 2002.

[9] S. Sampayan *et al.*, "Beam-target interaction experiments for bremsstrahlung converter applications," in *Proc. Part. Accel. Conf.*, Mar. 1999, pp. 1303–1305, doi: 10.1109/PAC.1999.795529.

[10] E. J. Lauer *et al.*, "Search for backstreaming ion defocusing during a single pulse of a 2 kA relativistic electron beam," in *Proc. 14th Int. Conf. High-Power Part. Beams (BEAMS)*, Albuquerque, NM, USA, Jun. 2002, pp. 248–251, doi: 10.1063/1.1530846.

[11] B. T. McCuistian, D. Moir, and L. Evan Rose, "Temporal spot size evolution of the DARHT first axis radiographic source," in *Proc. Epac*, Genoa, Italy, Jun. 2008, p. 1206.

[12] C. E. Crist *et al.*, "Time resolved, 2-D hard X-Ray imaging of relativistic electron-beam target interactions on ETA-II," in *Proc. 19th Int. Linear Accel. (LINA) Conf.*, Chicago, IL, USA, Nov. 1998, pp. 1–3. [Online]. Available: https://www.osti.gov/servlets/purl/291097

[13] C. Ekdahl, "Characterizing flash-radiography source spots," *J. Opt. Soc. Amer. A, Opt. Image Sci.*, vol. 28, no. 12, p. 2501, Dec. 2011, doi: 10.1364/josaa.28.002501.

[14] Y. Wang *et al.*, "Spot size measurement of a flash-radiography source using the pinhole imaging method," *Chin. Phys. C*, vol. 40, no. 7, Jul. 2016, Art. no. 076202, doi: 10.1088/1674-1137/40/7/076202.

[15] C. Aedy, S. Quillin, and A. D. J. Critchley, "A low cost time resolved spot diagnostic for flash X-ray machines," in *Proc. 31st IEEE Int. Conf. Plasma Sci. ICOPS IEEE Conf. Rec. Abstr.*, Jul. 2004, p. 282, doi: 10.1109/PLASMA.2004.1339939.

[16] J. Howorth, B. M. Ingle, P. Simpson, C. Aedy, and S. Quillin, "A low-cost time-resolved spot diagnostic for flash X-Ray machines," *Proc. SPIE*, vol. 5580, pp. 693–699, Mar. 2005, doi: 10.1117/12.58462.

[17] R. W. Bauer and R. C. Weingart, "Time-resolved fast-neutron pinhole camera for studying thermonuclear plasmas," California Univ., San Diego, CA, USA, Tech. Rep. UCRL-77527, 1976.

[18] K. Steinmetz, K. Hübner, J. P. Rager, and B. V. Robouch, "Neutron pinhole camera investigations on temporal and spatial structures of plasma focus neutron source," *Nucl. Fusion*, vol. 22, no. 1, pp. 30–32, Jan. 1982, doi: 10.1088/0029-5515/22/1/003.

[19] D. L. Fehl, R. J. Leeper, J. R. Lee, M. A. Hedemann, and W. A. Stygar, "A 1-D, hard X-Ray pinhole camera for flash X-Ray pulsed-power accelerators," in *Proc. 7th Pulsed Power Conf.*, Monterey, CA, USA, Jun. 1989, pp. 368–371, doi: 10.1109/PPC.1989.767500.

[20] D. L. Fehl *et al.*, "A one-dimensional time-resolved pinhole camera for intense pulsed bremsstrahlung sources," *Rev. Sci. Instrum.*, vol. 65, no. 6, pp. 1935–1948, Jun. 1994, doi: 10.1063/1.1144845.

[21] K. Masugata, E. Chishiro, N. Nakahama, K. Yatsui, and T. Tazima, "Conceptual design for a time resolved X-Ray imaging system useable in a strong hard X-ray background," *Rev. Sci. Instrum.*, vol. 68, no. 5, pp. 2046–2050, May 1997, doi: 10.1063/1.1148095.

[22] R. Richardson, G. Guethlein, S. Falabella, F. Chambers, B. Raymond, and J. Weir, "Time resolved X-Ray spot diagnostic," in *Proc. Part. Accel. Conf.*, Knoxville, TN, USA, May 2005, pp. 4302–4304, doi: 10.1109/PAC.2005.1591802.

[23] S. Lutz, D. Droemer, D. Devore, D. Rovang, S. Portillo, and J. Maenchen, "Development of a dynamic spot size diagnostic for flash radiographic X-ray sources," in *Dig. Tech. Papers. PPC 14th IEEE Int. Pulsed Power Conf.*, vol. 1, Jun. 2003, pp. 197–200, doi: 10.1109/PPC.2003.1277691.

[24] S. Portillo *et al.*, "Time-resolved spot size measurements from various radiographic diodes on the RITS-3 accelerator," *IEEE Trans. Plasma Sci.*, vol. 34, no. 5, pp. 1908–1913, Oct. 2006, doi: 10.1109/TPS.2006.883343.

[25] Y. Trunev *et al.*, "Influence of backstreaming ions on spot size of 2 MeV electron beam," *Laser Part. Beams*, vol. 37, no. 1, pp. 159–164, Mar. 2019, doi: 10.1017/s0263034619000314.

[26] P. V. Logachev *et al.*, "LIU-2 linear induction accelerator," *Instrum. Experim. Techn.*, vol. 56, no. 6, pp. 672–679, Nov. 2013, doi: 10.1134/s0020441213060195.

[27] T. J. Williams, "Axial energy distribution in disc-shaped tantalum and aluminium bremsstrahlung conversion targets," *Acta Phys. Polonica A*, vol. 115, no. 6, pp. 1180–1182, Jun. 2009, doi: 10.12693/APhysPolA.115.1180.

[28] M. A. Clift, R. A. Sutton, and D. V. Webb, "Dealing with cerenkov radiation generated in organic scintillator dosimeters by bremsstrahlung beams," *Phys. Med. Biol.*, vol. 45, no. 5, pp. 1165–1182, May 2000, doi: 10.1088/0031-9155/45/5/307.

Yu. A. Trunev received the B.S. and M.S. degrees in plasma physics from Novosibirsk State University, Novosibirsk, Russia, in 2003 and 2005, respectively.

He became a Junior Researcher with the Plasma Laboratory, Budker Institute of Nuclear Physics, Novosibirsk, in 2006. He was involved in electron beams, plasmas in an open magnetic trap. He is currently a Researcher with the Budker Institute of Nuclear Physics. His current research interests include high-power electron beams, beam diagnostics, beam-plasma physics.

D. I. Skovorodin received the Ph.D. degree in plasma physics from the Budker Institute of Nuclear Physics, Novosibirsk, Russia, in 2014.

He is currently a Senior Researcher with the Budker Institute of Nuclear Physics. He has been involved in theory and experiments for fusion linear magnetic systems development and high power electron beam science.

A. V. Burdakov, photograph and biography not available at the time of publication.

S. S. Popov received the Ph.D. degree in plasma physics from the Budker Institute of Nuclear physics, Novosibirsk, Russia, in 2009.

He is currently a Senior Researcher with the Budker Institute of Nuclear Physics. His main scientific interests are optical diagnostics of plasma, laser physics, and nonlinear dynamics.

P. A. Kolesnikov, photograph and biography not available at the time of publication.

V. V. Danilov received the B.S. degree in accelerators physics and the M.S. degree in plasma physics from Novosibirsk State University, Novosibirsk, Russia, in 2016 and 2018, respectively.

He became a Research Assistant with the Budker Institute of Nuclear Physics, Novosibirsk, in 2018. His current research interests include high power electron beams, X-ray diagnostic development, and plasma diagnostics.

V. V. Kurkuchekov received the bachelor's and master's degrees in plasma physics from Novosibirsk State University, Novosibirsk, Russia, in 2010 and 2012, respectively.

He is currently a Researcher with the Budker Institute of Nuclear Physics, Novosibirsk, where he is involved in fusion and high power electron beams science. At the moment his research interests include electron beam development and diagnostics, X-ray diagnostics development.

M. G. Atlukhanov received the bachelor's and master's degree in physics from Novosibirsk State Technical University, Novosibirsk, Russia, in 2010 and 2012, respectively.

He is currently a Researcher with the Budker Institute of Nuclear Physics, Novosibirsk. He is involved in the diagnosis and neutralization of negative ion beams. His current research interests include photoneutralization on base of nonresonance adiabatic trap of photons and noninvasive methods for diagnostics negative ion beams, and X-ray diagnostic.

I. V. Kulenko, photograph and biography not available at the time of publication.

A. S. Arakcheev, photograph and biography not available at the time of publication.

V. T. Astrelin, photograph and biography not available at the time of publication.

S. L. Sinitsky, photograph and biography not available at the time of publication.

A. A. Starostenko, photograph and biography not available at the time of publication.

D. A. Starostenko, photograph and biography not available at the time of publication.

O. A. Nikitin, photograph and biography not available at the time of publication.

V. Yu. Politov, photograph and biography not available at the time of publication.

E. S. Lee, photograph and biography not available at the time of publication.